INORGANIC CHEMISTRY FRONTIERS

RESEARCH ARTICLE

View Article Online
View Journal | View Issue

Cite this: *Inorg. Chem. Front.*, 2025, **12**, 4911

$Na_2PbB_6O_{10}SO_4$ and $Ca_{2.58}Pb_{0.42}B_6O_{11}SO_4$: first borate–sulfates featuring 3D porous borate anionic frameworks†

Huan Pei,‡[a] Zijian Li,‡[b] Shaohua Liu,[b] Xueling Hou *[b] and Fangfang Zhang *[b]

Received 9th February 2025,
Accepted 2nd April 2025

DOI: 10.1039/d5qi00394f

rsc.li/frontiers-inorganic

This study presents two new borate–sulfate compounds, $Na_2PbB_6O_{10}SO_4$ (**I**) and $Ca_{2.58}Pb_{0.42}B_6O_{11}SO_4$ (**II**). Both crystals form unique three-dimensional (3D) porous frameworks $^3[B6O10]_\infty$ and $^3[B7O13]_\infty$, composed of fundamental building blocks $[B_6O_{13}]$ and $[B_7O_{17}]$, respectively, with $[SO_4]$ units embedded within the pores. These examples represent the first observation of 3D borate frameworks in borate–sulfates, thus expanding the structural diversity of borate–sulfate compounds. The relationship between the structure and birefringence was studied using first-principles calculations. This study uncovers new insights into the connectivity and structural properties of borate–sulfates.

1. Introduction

Borates have attracted considerable scientific attention due to their remarkable structural diversity and exceptional optical properties.[1–16] This structural diversity arises from the versatile coordination of the boron atom, which can form $[BO_2]$, $[BO_3]$, and $[BO_4]$ units with two, three, or four oxygen atoms, respectively.[17–28] These basic units can exist in isolation or assemble into complex fundamental building blocks (FBBs), which further polymerize into diverse borate structures, including 0D clusters, 1D chains, 2D layers, and 3D frameworks.[29–34] From the perspective of optical properties, the B–O groups are characterized by a large HOMO–LUMO gap and are beneficial for developing ultraviolet (UV) materials with wide band gaps.[35] Specifically, the π-conjugated $[BO_3]$ groups, known for their high hyperpolarizability and pronounced polarizability anisotropy, are highly desirable components for designing nonlinear optical (NLO) and birefringent materials.[36–38]

In the realm of mixed anionic compounds, borosulfates and borate–sulfates are characterized by their rich structural chemistry and fascinating physicochemical properties.[39–43] Borosulfates are characterized by condensed tetrahedral $[BO_4]$ and $[SO_4]$ units interconnected through B–O–S linkages, forming oxoanionic frameworks that resemble silicates.[44–48] Since the first synthesis of $K_5[B(SO_4)_4]$[48] in 2012, over 50 borosulfates have been reported. In contrast, in borate–sulfates, the borate anions and sulfate anions are not directly connected.[41,42,49–51] To the best of our knowledge, only 26 borate–sulfates have been identified (as summarized in Table S1†). As shown in Fig. 1, the S–O groups in borate–sulfates exist as isolated $[SO_4]$ units, while the B–O groups can form isolated $[BO_3]$ or $[BO_4]$ units, one-dimensional B–O chains, or two-dimensional B–O layers. To date, no borate–sulfates with three-dimensional B–O frameworks have been reported.

Owing to the limited systematic exploration of structure–property relationships in borate–sulfates, expanding this family of compounds and uncovering their unique features are essential. In this study, we report two new borate–sulfate compounds, $Na_2PbB_6O_{10}SO_4$ (**I**) and $Ca_{2.58}Pb_{0.42}B_6O_{11}SO_4$ (**II**). These compounds represent the first reported examples of borate–sulfates featuring 3D porous borate anionic frameworks (structurally porous frameworks with crystallographically defined channels). The unique structures of the two compounds, as well as their structural changes, are thoroughly discussed. Pure phases were obtained, and their thermal, infrared, and UV-Vis-NIR diffuse reflectance spectroscopy properties were comprehensively characterized. First-principles calculations were employed to systematically analyze the optical properties of these compounds, revealing the intrinsic

[a]*Key Laboratory for Green Processing of Chemical Engineering of XinjiangBingtuan, School of Chemistry and Chemical Engineering, Shihezi University, Shihezi 832003, China*

[b]*Research Center for Crystal Materials; Key Laboratory of Functional Materials and Devices for Special Environmental Conditions; Xinjiang Key Laboratory of Functional Crystal Materials; Xinjiang Technical Institute of Physics and Chemistry, Chinese Academy of Sciences, 40-1 South Beijing Road, Urumqi 830011, China.*
E-mail: xlhou@ms.xjb.ac.cn, ffzhang@ms.xjb.ac.cn

†Electronic supplementary information (ESI) available. CCDC 2386130 and 2386131. For ESI and crystallographic data in CIF or other electronic format see DOI: https://doi.org/10.1039/d5qi00394f

‡These authors contributed equally to this work.

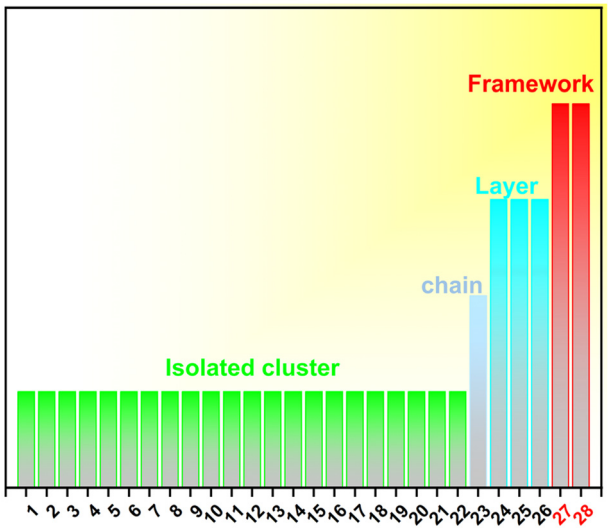

Fig. 1 Classification of compounds based on the dimensionality of the constituent borate groups. It should be noted that the number of compounds corresponds to those in Table S1.† Data were derived from the Inorganic Crystal Structure Database (ICSD, Version 5.2.0, Data Release 2025.1).

relationship between birefringence and the density of $[BO_3]$ units.

2. Experimental section

2.1 Materials

The starting materials used in this study included Na_2SO_4 (≥99.0%), which was supplied by Tianjin Xinbote Chemical Co. Ltd, PbO (99.97%) and B_2O_3 (99.9%) were obtained from Shanghai Aladdin Biochemical Technology Co. Ltd, and $CaSO_4$ (97.0%) was purchased from Macklin. All materials were used as received without further purification.

2.2 Synthesis

Single crystals of **I** and **II** were grown using the high-temperature solution method in a vacuum-sealed system. For **I**, a mixture of Na_2SO_4 (0.142 g, 1 mmol), PbO (0.223 g, 1 mmol), and B_2O_3 (0.209 g, 3 mmol) was loaded into a silica glass tube (∅ 10 mm × 20 cm), which was flame-sealed under a vacuum of 10^{-3} Pa. For **II**, a mixture of $CaSO_4$ (0.351 g, 2.58 mmol), PbO (0.094 g, 0.42 mmol), and B_2O_3 (0.209 g, 3 mmol) was loaded and sealed similarly. The sealed tubes were heated to 450 °C over 10 hours, annealed at this temperature for 24 hours, cooled to 300 °C at a rate of 1 °C h^{-1}, and then cooled to room temperature at a rate of 10 °C h^{-1}. Polycrystalline powder samples of **I** and **II** were synthesized using the same method as described above for the single crystals. Colorless transparent block-shaped microcrystals were obtained, with a yield of approximately 94% based on Na for **I** and a yield of approximately 90% based on Ca for **II**.

3. Results and discussion

3.1 Crystal structure

3.1.1 Structures of I. **I** crystallizes in the space group *Pnma*, with detailed crystallographic data provided in Table S2 in the ESI.† The asymmetric unit comprises two Na, one Pb, four B, one S, and nine O atoms in crystallographically unique positions (Fig. S1a†). The boron atoms exhibit two distinct coordination environments: B(1) forms a $[BO_3]$ triangular unit, while B(2), B(3), and B(4) form $[BO_4]$ tetrahedral units. Three $[BO_4]$ tetrahedra share a corner through the μ_3-O9 atom, connecting to three $[BO_3]$ units and forming a compact $[B_6O_{13}]$ cluster (Fig. 2a) as the FBB of the structure. The $[B_6O_{13}]$ FBB can be represented as $\{6: [(6:3\Delta + 3T)]\}$, which is also present in $NH_4NaB_6O_{10}$.[52] The $[B_6O_{13}]$ units form a boron–oxygen framework featuring 16-, 18-, and 20-membered rings (MRs) *via* shared O atoms. These rings form an irregular hexahedron, measuring 10.13 Å × 6.67 Å, 7.34 Å × 7.02 Å, and 7.02 Å × 4.59 Å (Fig. 2b). Each $[B_6O_{13}]$ unit acts as a 6-connected node, connecting to six neighboring units through shared O atoms, forming a 3D framework with a pcu topology and the Schläfli symbol $(4^{12}\cdot6^3)$ (Fig. 2c). The $[B_6O_{13}]$ FBBs form a three-dimensional structure of $^3{}_\infty[B_6O_{10}]$ by sharing O atoms, which is clearly depicted in Fig. 2d. The $[SO_4]^{2-}$ ions are uniformly distributed within the porous framework, creating a stable and well-organized ionic arrangement (Fig. 2d). The B–O bond lengths range from 1.358(7) to 1.365(7) Å in $[BO_3]$ units to 1.356(10) to 1.525(6) Å in $[BO_4]$ units. The S–O bond lengths of $[SO_4]$ tetrahedra range from 1.458(7) to 1.472(7) Å. The O–B–O bond angles range from 106.45(5) to 122.5(5)° and the O–S–O bond angles range from 108.9(4) to 110.4(4)°. Na and Pb cation coordination environments are depicted in Fig. S2a,† with Na–O bond lengths of 2.295(4)–2.710(4) Å and Pb–O bond lengths of 2.604(6)–2.736(5) Å. Bond valence sum (BVS) calculations validate oxidation states as −2 (O), +3 (B), +6 (S), +2 (Pb), and +1 (Na) (Table S3, ESI†), which are consistent with their respective oxidation states. Selected bond lengths and angles are listed in Table S4 of the ESI.†

3.1.2 Structures of II. **II** crystallizes in the space group *P*21/*c*, with relevant crystallographic data provided in Table S2 of the ESI.† In the asymmetric unit, the Ca/Pb, B, S, and O atoms occupy 3, 6, 1, and 15 crystallographically unique positions, respectively (Fig. S1b†). B(1) forms a $[BO_3]$ triangular unit, while B(2)–B(6) form $[BO_4]$ tetrahedra. Three $[BO_4]$ tetrahedra are interconnected *via* a shared μ_3-O6 atom and further linked to three adjacent $[BO_4]$ units, with B(2) and B(3) connected through the B(1)O_3 triangle. This arrangement forms a new compact $[B_7O_{17}]$ cluster (Fig. 2e), which serves as the FBB. The $[B_7O_{17}]$ FBB can be expressed as $\{7: [(7:\Delta + 6T)]\}$. Fig. 2f and g depict the unique 3D porous borate anionic framework of **II**, featuring a porous structure composed of boron–oxygen rings with 16-, 18-, and 24-MR configurations. The framework features three asymmetric faces with dimensions of 6.18 Å × 4.00 Å, 7.54 Å × 3.11 Å, and 11.62 Å × 6.66 Å, resulting in the formation of a regular hexagonal pore geometry. As depicted in Fig. 2g, the structure is composed of 12 $[B_7O_{17}]$ clusters.

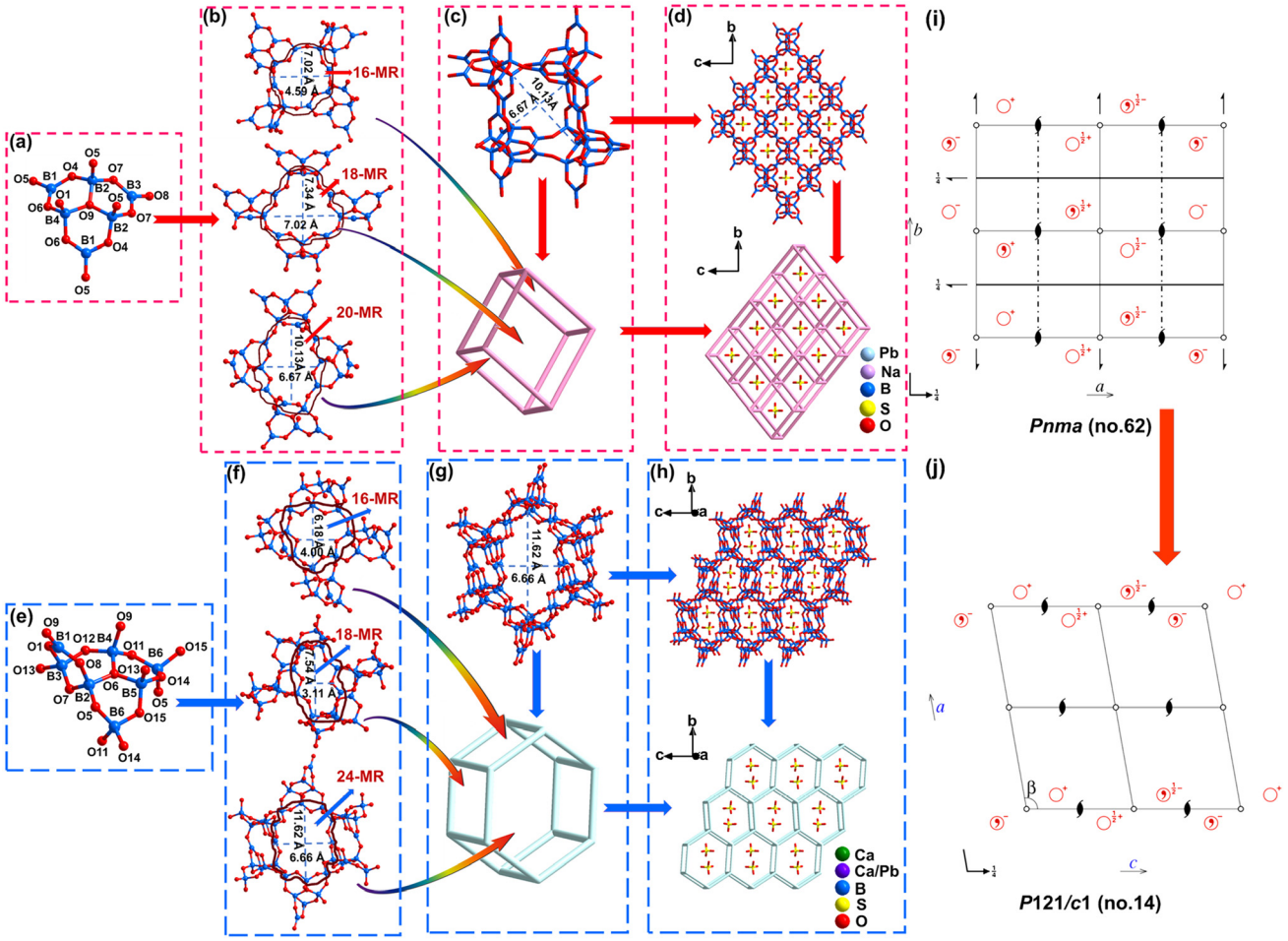

Fig. 2 (a and e) The $[B_6O_{13}]$ and $[B_7O_{17}]$ FBBs of structures **I** and **II**; (b and f) 16-, 18-, and 20-MRs formed by $[B_6O_{13}]$ in **I**; 16-, 18-, and 24-MRs formed by $[B_7O_{17}]$ in **II**; (c and g) frameworks constructed from interconnected ring structures in **I** and **II**; (d and h) view of the topology network in **I** and **II**; (i and j) spatial symmetry operation change from **I** [high symmetry *Pnma* (no. 62)] to **II** [low symmetry *P*21/*c* (no. 14)].

Each $[B_7O_{17}]$ unit acts as a 5-connected node, linking to five neighboring clusters *via* shared O atoms (Fig. 2g). The resulting 3D framework adopts a pcu topology with the Schläfli symbol $(4^6{\cdot}6^4)$ (Fig. 2g). Furthermore, the $[B_7O_{17}]$ FBBs form a 3D structure of $^3{}_\infty[B_7O_{13}]$ through the sharing of O atoms.

These linkages create a unique 3D porous borate anionic framework with open pores along the *bc* directions (Fig. 2h). The $[SO_4]^{2-}$ ions are embedded within the porous structure (Fig. 2h). The B–O bond lengths within the $[BO_3]$ triangles range from 1.353(3) to 1.369(3) Å, while those in the $[BO_4]$ tetrahedra range from 1.420(3) to 1.574(3) Å. The S–O bond lengths within the $[SO_4]$ tetrahedra vary from 1.4611(18) to 1.4861(19) Å. The O–B–O bond angles span from 102.36(17) to 120.8(2)°, while the O–S–O bond angles range from 107.40(10) to 111.89(12)°. The coordination environments of the Ca and Pb cations are shown in Fig. S2b of the ESI.† The Ca–O bond lengths range from 2.2844(15) to 2.877(2) Å, while the Pb–O bond lengths range from 2.4921(16) to 2.7899(19) Å. BVS calculations confirm the oxidation states of O, B, S, Pb, and Ca as −2, +3, +6, +2, and +2, respectively, as summarized in Table S3 of the ESI,† and these oxidation states are consistent with the known oxidation states. Selected bond lengths and angles are provided in Table S4 of the ESI.†

3.2 Comparative structural analysis of compounds I and II

The structural comparison between **I** and **II** is primarily driven by the substitution of Na^+ with Ca^{2+}, resulting in significant changes in the crystal framework. Owing to the difference in cations, the structural comparison between **I** and **II** reveals a reduction in the symmetry of the space group, shifting from a higher-symmetry group (*Pnma*) to a lower-symmetry group ($P2_1/c$) (Fig. 2i and j). The Na^+ cations, with shorter coordination bonds (2.295–2.710 Å), support a compact and ordered framework.

In contrast, **II** incorporates Ca^{2+}, which exhibits stronger and more flexible coordination (Ca–O bond lengths: 2.284–2.877 Å), facilitating the formation of larger and more complex $[B_7O_{17}]$ clusters. The Ca^{2+}-driven transition also results in a shift from a 6-connected to 5-connected topology, along with longer B–O and S–O bond lengths and wider O–B–

O bond angles. Overall, the transition from **I** to **II** is attributed to the higher charge density and larger coordination capacity of Ca^{2+}, which enables increased structural flexibility, the formation of more complex clusters, and reorganization of the 3D porous borate anionic framework. This comparison highlights the critical role of cation substitution in tuning crystal topology and framework properties.

3.3 Characterization

Elemental analysis by energy-dispersive X-ray spectroscopy (EDS) revealed the presence of Na, Pb, B, S, and O in compound **I** and Ca, Pb, B, S, and O in compound **II** (see ESI Fig. S3a and b†). The purity of the polycrystalline sample was confirmed using powder XRD analysis (Fig. 3a and b). The IR spectra were recorded to confirm the coordination environment of B and S atoms, suggesting the presence of triangular [BO_3], tetrahedral [BO_4], and [SO_4] groups. The absence of vibration bands near 3500 cm^{-1} confirms that hydroxyl groups are not present in the structure (Fig. 3c and d; Table S5†). Based on previous studies,[46,53] the asymmetric (ν_{asym}) and symmetric (ν_{sym}) stretching vibrations of the [BO_3] units are detected at 1300–1531 and 910–945 cm^{-1}, respectively. The vibrational peaks at 805–871 and 528–592 cm^{-1} are attributed to the out-of-plane bending [δ(O–B–O)] modes of the [BO_3] groups. The ν_{sym} of the [BO_4] tetrahedra are observed between 1103 and 1130 cm^{-1}. The very strong band at around 1195–1200 cm^{-1} can be ascribed to the ν_{asym} of the [SO_4] units. The ν_{sym} of the [SO_4] units are observed at around 505–509 cm^{-1}. Detailed peak assignments for the IR spectra are provided in Table S5 of the ESI.† Thermogravimetric-differential scanning calorimetry (TG-DSC) analysis was performed to study the thermal behavior. The results show that **I** and **II** are thermally stable up to 610 and 750 °C, respectively. Beyond these temperatures, decomposition occurs, accompanied by significant weight loss. This decomposition corresponds to the endothermic peaks at 640 and 774 °C on the DSC curves (Fig. 3e and f). Therefore, **I** and **II** exhibit excellent thermal stability below 640 and 774 °C, making them suitable for use in a wide range of thermal applications. The UV-Vis-NIR spectra of compounds **I** and **II** show absorption ranges of 270–1200 nm and 300–1200 nm, respectively. Fig. S4a and b† indicate that the UV cut-off edges are below 270 nm for **I** (with 5% reflectance) and below 300 nm for **II** (with 47% reflectance).

3.4 First-principles calculations

The electronic structures and optical properties were calculated by the first-principles method for **I** and **II**.

The band structure calculations performed using the generalized gradient approximation (GGA)[54] show a direct bandgap of 4.83 eV for **I** and an indirect bandgap of 4.48 eV for **II**, respectively (Fig. 4a and b). From the total and partial densities of states (DOS and PDOS) of **I** (Fig. 4c), the highest states of the valence bands (VBs) are primarily dominated by O 2p orbitals, while the lowest states of the conduction bands (CBs) are mainly derived from B 2p and Pb 6p orbitals, with a minor contribution from Na 3s and 3p orbitals. In the vicinity of the Fermi level in **II** (Fig. 4d), O 2p mostly occupies the VBs, while B 2p and Pb 6p orbitals dominate the CBs; additionally, the Ca 3d and S 3p orbitals contribute a minor portion. As O 2p and B 2p orbitals have apparent interactions in the VB and CB regions, it can be concluded that the band gap and linear optical performance are determined by the B–O framework in **I** and **II**.

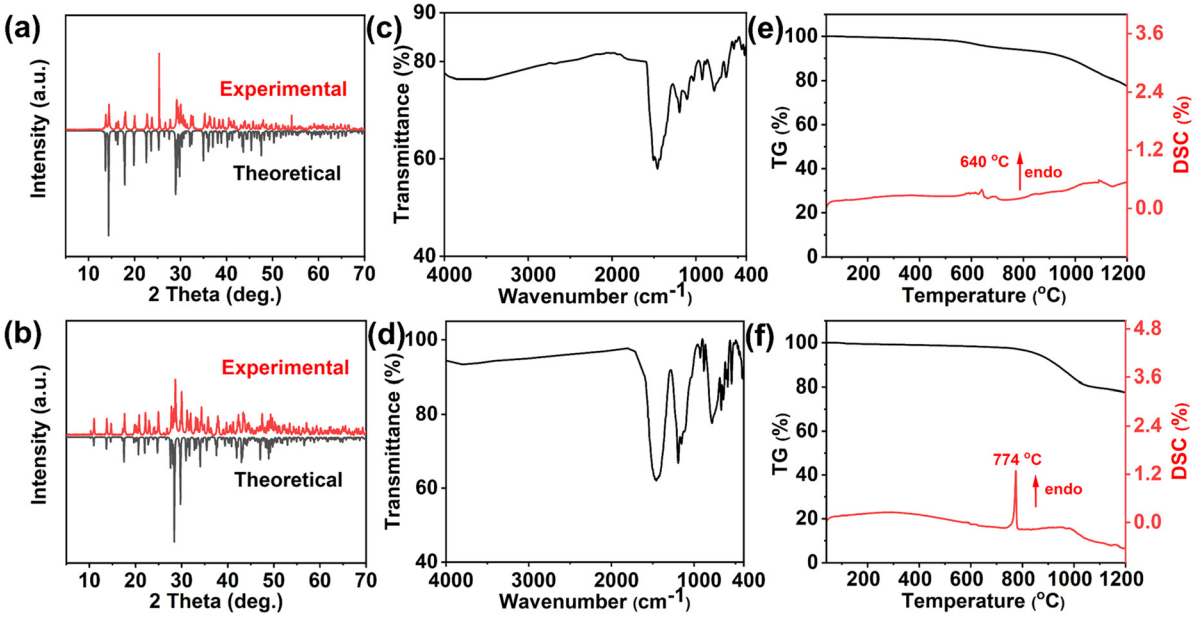

Fig. 3 Performance of **I** and **II**. (a and b) Experimental and calculated XRD patterns; (c and d) IR spectra; (e and f) TG-DSC curves.

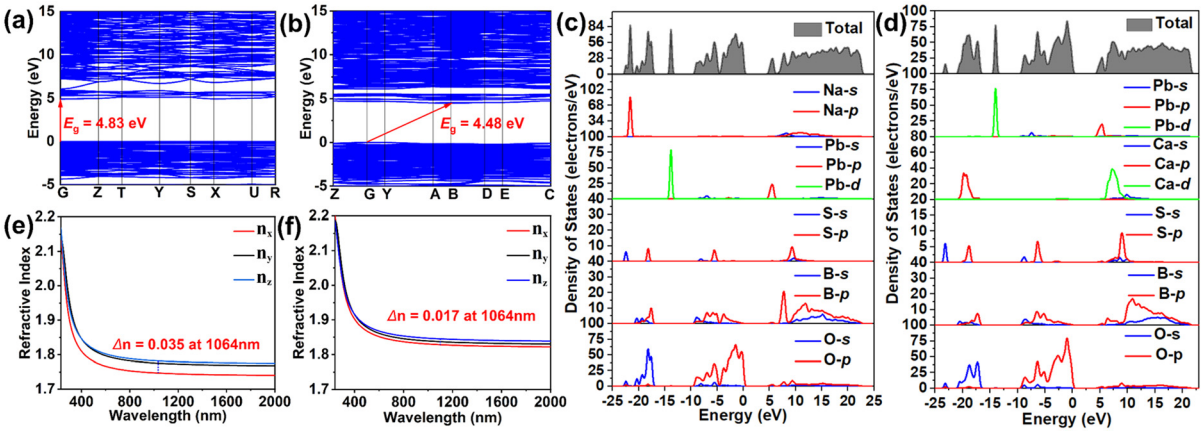

Fig. 4 Theoretical calculations of **I** and **II**. (a and b) Electronic band structures based on GGA. (c and d) Total and partial densities of states. (e and f) Calculated refractive index curves. (a, c, and e) and (b, d, and f) **I** and **II**, respectively.

The refractive indices of **I** and **II** were calculated using the first-principles method (Fig. 4e and f). The calculated birefringence is about 0.035 and 0.017 at 1064 nm for **I** and **II**, respectively. To further understand the structure–optical property relationship of the above-mentioned materials, the spatial density of the [BO_3] groups was also calculated (Table S6†). The relationship between the birefringence of **I** and **II** with the density was determined. While comparing structures **I** and **II**, it can be seen that the anion [BO_3] density in **I** is higher, resulting in greater birefringence in **I** than in **II**. The origin of birefringence was analyzed using the response electron distribution anisotropy (REDA) method.[55] As shown in Table S7,† the [BO_3] units contribute significantly, with a proportion of 77.0%, while the [BO_4], [SO_4], [$Na1O_8$], [$Na2O_6$], and [PbO_9] units contribute smaller proportions of −12.2, 3.0, 7.9, 10.7, and 13.7% in **I**, respectively. The contribution of the [BO_3] units is 62.4%, and the contributions of the [BO_4], [SO_4], [$Na1O_8$], [$Na2O_6$], and [PbO_9] units are 13.5, 9.6, 6.4, 13.5, and −5.4% for **II**, respectively. Since the [BO_3] unit has larger polarizability anisotropy,[38] and the density of the [BO_3] units in **I** is higher than that in **II**, the birefringence of **I** is greater than that of **II**.

4. Conclusion

In summary, two new borate–sulfates, $Na_2PbB_6O_{10}SO_4$ (**I**) and $Ca_{2.58}Pb_{0.42}B_6O_{11}SO_4$ (**II**), were successfully synthesized and characterized. Both compounds feature novel 3D porous borate anionic frameworks that incorporate isolated [SO_4] groups. The transition from **I** to **II** is driven by differences in cationic radii, leading to distinct 3D porous borate anionic frameworks. First-principles calculations reveal that the birefringence of **I** is significantly greater than that of **II**, which can be attributed to the higher density of [BO_3] units in **I**. These findings offer new insights into the structural diversity and connectivity of borate and sulfate groups, paving the way for further exploration of their functional and structural properties.

Author contributions

Fangfang Zhang supervised the research and revision of the manuscript. Huan Pei designed and performed the experiments, wrote the first draft, and revised it. Shaohua Liu did the theoretical calculations. Zijian Li assisted with the experimental work. All authors participated in the discussion.

Data availability

Computational procedures, crystal data information, bond valence sum, selected bond lengths, and angles are available in the article and its ESI.†

Conflicts of interest

The authors declare no conflicts of interest.

Acknowledgements

This work was supported by the Tianshan Innovation Team (2022TSYCTD0005) and the Strategic Priority Research Program of the Chinese Academy of Sciences (XDB0880000).

References

1 M. Mutailipu, K. R. Poeppelmeier and S. Pan, Borates: A Rich Source for Optical Materials, *Chem. Rev.*, 2021, **121**, 1130–1202.
2 Z. Yan, J. Fan, S. Pan and M. Zhang, Recent Advances in Rational Structure Design for Nonlinear Optical Crystals:

Leveraging Advantageous Templates, *Chem. Soc. Rev.*, 2024, **53**, 6568–6599.
3 C. T. Chen, T. Sasaki, R. K. Li, Y. C. Wu, Z. S. Lin, Y. Mori, Z. G. Hu, J. Y. Wang, S. Uda, M. Yoshimura and Y. Kaneda, *Borate Crystals for Nonlinear Optical Applications: principals and applications*, Wiley-VCH Weinheim, 2012.
4 T. T. Tran, H. Yu, J. M. Rondinelli, K. R. Poeppelmeier and P. S. Halasyamani, Deep Ultraviolet Nonlinear Optical Materials, *Chem. Mater.*, 2016, **28**, 5238–5258.
5 A. Tudi, S. Han, Z. Yang and S. Pan, Potential Optical Functional Crystals with Large Birefringence: Recent Advances and Future Prospects, *Coord. Chem. Rev.*, 2022, **459**, 214380.
6 C. Chen, Y. Wang, B. Wu, K. Wu, W. Zeng and L. Yu, Design and synthesis of an ultraviolet-transparent nonlinear optical crystal $Sr_2Be_2B_2O_7$, *Nature*, 1995, **373**, 322–324.
7 F. Li, W. Jin, R. An, M. Mutailipu, S. Pan and Z. Yang, Covalently Bonded Fluorine Optimizing Deep-Ultraviolet Nonlinear Optical Performance of Fluorooxoborates, *Sci. Bull.*, 2024, **69**, 1192–1196.
8 A. Tudi, S. Han, Z. Yang and S. Pan, Potential Optical Functional Crystals with Large Birefringence: Recent Advances and Future Prospects, *Coord. Chem. Rev.*, 2022, **459**, 214380.
9 T. T. Tran, N. Z. Koocher, J. M. Rondinelli and P. S. Halasyamani, Beryllium-Free β-$Rb_2Al_2B_2O_7$ as a Possible Deep-Ultraviolet Nonlinear Optical Material Replacement for $KBe_2BO_3F_2$, *Angew. Chem., Int. Ed.*, 2017, **56**, 2969–2973, (*Angew. Chem.*, 2017, **129**, 3015–3019).
10 T. T. Tran, H. Yu, J. M. Rondinelli, K. R. Poeppelmeier and P. S. Halasyamani, Deep Ultraviolet Nonlinear Optical Materials, *Chem. Mater.*, 2016, **28**, 5238–5258.
11 C. T. Chen, B. C. Wu, A. D. Jiang and G. M. You, A new ultraviolet SHG crystal—β-BaB_2O_4, *Sci. Sin. Ser. B*, 1985, **28**, 235.
12 Q. Zhang, R. An, X. Long, Z. Yang, S. Pan and Y. Yang, Exploiting Deep-Ultraviolet Nonlinear Optical Materials $Rb_2ScB_3O_6F_2$ Originated from Congruously Oriented $[B_3O_6]$ Groups, *Angew. Chem., Int. Ed.*, 2025, **64**, e202415066.
13 C. T. Chen and G. Liu, Recent Advances in Nonlinear Optical and Electro-Optical Materials, *Annu. Rev. Mater. Sci.*, 1986, **16**, 203.
14 J. Jiao, M. Zhang and S. Pan, Aluminoborates as Nonlinear Optical Materials, *Angew. Chem., Int. Ed.*, 2023, **62**, e202217037.
15 M. Mutailipu and S. Pan, Emergent Deep-Ultraviolet Nonlinear Optical Candidates, *Angew. Chem., Int. Ed.*, 2020, **59**, 20302–20317.
16 X. Wang, Y. Wang, B. Zhang, F. Zhang, Z. Yang and S. Pan, CsB4O6F: A Congruent-melting deep-Ultraviolet Nonlinear Optical Material by Combining Superior Functional Units, *Angew. Chem., Int. Ed.*, 2017, **56**, 14119–14123.
17 C. Calvo and R. Faggiani, Linear metaborate anions, BO_2^-, in apatitic phosphates, *J. Chem. Soc., Chem. Commun.*, 1974, **17**, 714–715.
18 H. A. Höppe, $Gd_4(BO_2)O_5F$ – a gadolinium borate fluoride oxide comprising a linear BO_2 moiety, *Z. Naturforsch.*, 2015, **70**(11), 769–774.
19 C. Huang, M. Mutailipu, F. Zhang, K. J. Griffith, C. Hu, Z. Yang, J. M. Griffin, K. R. Poeppelmeier and S. Pan, Expanding the chemistry of borates with functional $[BO_2]^-$ anions, *Nat. Commun.*, 2021, **12**, 2597.
20 Y. Zhang, F. Li, R. Yang, Y. Yang, F. Zhang, Z. Yang and S. Pan, $Rb_5Ba_2(B_{10}O_{17})_2(BO_2)$: The formation of unusual functional $[BO_2]^-$ in borates with deep-ultraviolet transmission window, *Sci. China:Chem.*, 2022, **65**, 719–725.
21 R. Liu, H. Wu, H. Yu, Z. Hu, J. Wang and Y. Wu, K5Mg2La3(BO3)6: An Efficient, Deep-Ultraviolet Nonlinear Optical Material, *Chem. Mater.*, 2021, **33**, 4240–4246.
22 S. Zhao, P. Gong, L. Bai, X. Xu, S. Zhang, Z. Sun, Z. Lin, M. Hong, C. Chen and J. Luo, Beryllium-free $Li_4Sr(BO_3)_2$ for deep-ultraviolet nonlinear optical applications, *Nat. Commun.*, 2014, **5**, 4019.
23 M. Mutailipu, M. Zhang, H. Li, X. Fan, Z. Yang, S. Jin, G. Wang and S. Pan, $Li_4Na_2CsB_7O_{14}$: a new edge-sharing $[BO_4]^{5-}$ tetrahedra containing borate with high anisotropic thermal expansion, *Chem. Commun.*, 2019, **55**, 1295–1298.
24 X. Wang, F. Zhang, L. Gao, Z. Yang and S. Pan, Nontoxic KBBF Family Member $Zn_2BO_3(OH)$: Balance between Beneficial Layered Structure and Layer Tendency, *Adv. Sci.*, 2019, **6**, 1901679.
25 H. Yu, H. Wu, S. Pan, Z. Yang, X. Hou, X. Su, Q. Jing, K. R. Poeppelmeier and J. M. Rondinelli, $Cs_3Zn_6B_9O_{21}$: A Chemically Benign Member of the KBBF Family Exhibiting the Largest Second Harmonic Generation Response, *J. Am. Chem. Soc.*, 2014, **136**, 1264–1267.
26 W. Zhang, Z. Zhang, W. Jin, R. Zhang, M. Cheng, Z. Yang and S. Pan, From borophosphate to fluoroborophosphate: a rational design of fluorine-induced birefringence enhancement, *Sci. China:Chem.*, 2021, **64**, 1498–1503.
27 Z. Li, W. Jin, F. Zhang, Z. Yang and S. Pan, Exploring Short-Wavelength Phase-Matching Nonlinear Optical Crystals by Employing $KBe_2BO_3F_2$ as the Template, *ACS Cent. Sci.*, 2022, **8**, 1557–1564.
28 X. Chen, B. Zhang, F. Zhang, Y. Wang, M. Zhang, Z. Yang, K. R. Poeppelmeier and S. Pan, Designing an Excellent Deep-Ultraviolet Birefringent Material for Light Polarization, *J. Am. Chem. Soc.*, 2018, **140**, 16311–16319.
29 H. Pei, L. Zhang, H. Cheng, S. Wang, Z. Yang, F. Zhang and S. Pan, Structural Evolution and Optical Properties of Hydroxyfluorooxoborates $MM'_{2n-1}[B_3O_3F_4(OH)]_n$ (M = K, Cs, and Rb; M′ = K, NH_4, and Cs; n = 1, 2, and 3), *Chem. Mater.*, 2024, **36**, 11697–11705.
30 F. Zhang, X. Chen, M. Zhang, W. Jin, S. Han, Z. Yang and S. Pan, An excellent deep-ultraviolet birefringent material based on $[BO_2]_\infty$ infinite chains, *Light:Sci. Appl.*, 2022, **11**, 252.
31 H. Pei, X. Wang, J. Zhang, F. Zhang, Z. Yang and S. Pan, $Ba_2B_9O_{13}F_4{\cdot}BF_4$: first fluorooxoborate with unprecedented infinite $[B_{18}O_{26}F_8]$ tubes and deep-ultraviolet cutoff edge, *Sci. China:Chem.*, 2023, **66**, 1073–1077.

32 M. Mutailipu, M. Zhang, H. Wu, Z. Yang, Y. Shen, J. Sun and S. Pan, $Ba_3Mg_3(BO_3)_3F_3$ polymorphs with reversible phase transition and high performances as ultraviolet nonlinear optical materials, *Nat. Commun.*, 2018, **9**, 3089.

33 Y. Wang, B. Zhang, Z. Yang and S. Pan, Cation-Tuned Synthesis of Fluorooxoborates: Towards Optimal Deep-Ultraviolet Nonlinear Optical Materials, *Angew. Chem., Int. Ed.*, 2018, **57**, 2150–2154.

34 H. Liu, H. Wu, Z. Hu, J. Wang, Y. Wu and H. Yu, $Cs_3[(BOP)_2(B_3O_7)_3]$: A Deep-Ultraviolet Nonlinear Optical Crystal Designed by Optimizing Matching of Cation and Anion Groups, *J. Am. Chem. Soc.*, 2023, **145**, 12691–12700.

35 B. Zhang, G. Shi, Z. Yang, F. Zhang and S. Pan, Fluorooxoborates: Beryllium-Free Deep-Ultraviolet Nonlinear Optical Materials without Layered Growth, *Angew. Chem., Int. Ed.*, 2017, **56**, 3916–3919.

36 M. Mutailipu, M. Zhang, Z. Yang and S. Pan, Targeting the Next Generation of Deep-Ultraviolet Nonlinear Optical Materials: Expanding from Borates to Borate Fluorides to Fluorooxoborates, *Acc. Chem. Res.*, 2019, **52**, 791–801.

37 B. Lei, S. Pan, Z. Yang, C. Cao and D. J. Singh, Second Harmonic Generation Susceptibilities from Symmetry Adapted Wannier Functions, *Phys. Rev. Lett.*, 2020, **125**, 187402.

38 G. Shi, Y. Wang, F. Zhang, B. Zhang, Z. Yang, X. Hou, S. Pan and K. R. Poeppelmeier, Finding the Next Deep-Ultraviolet Nonlinear Optical Material: $NH_4B_4O_6F$, *J. Am. Chem. Soc.*, 2017, **139**, 10645–10648.

39 Z. Li, W. Jin, F. Zhang, Z. Chen, Z. Yang and S. Pan, Achieving Short-Wavelength Phase-Matching Second Harmonic Generation in Boron-Rich Borosulfate with Planar $[BO_3]$ Units, *Angew. Chem., Int. Ed.*, 2022, **61**, e202112844.

40 Z. Li, W. Jin, F. Zhang, Z. Yang and S. Pan, Exploring Short-Wavelength Phase-Matching Nonlinear Optical Crystals by Employing $KBe_2BO_3F_2$ as the Template, *ACS Cent. Sci.*, 2022, **8**, 1557–1564.

41 W.-W. Wang, X. Xu, J.-T. Kong and J.-G. Mao, $RE(SO_4)[B(OH)_4](H_2O)$, $RE(SO_4)[B(OH)_4](H_2O)_2$, and $RE(SO_4)[B(OH)_4](H_2O)\cdot H_2O$: Rare-Earth Borate-Sulfates Featuring Three Types of Layered Structures, *Inorg. Chem.*, 2018, **57**, 163–174.

42 T.-T. Ruan, W.-W. Wang, C.-L. Hu, X. Xu and J.-G. Mao, $Pb_4(BO_3)_2(SO_4)$ and $Pb_2[(BO_2)(OH)](SO_4)$: New lead(II) borate-sulfate mixed-anion compounds with two types of 3D network structures, *J. Solid State Chem.*, 2018, **260**, 39–45.

43 L. C. Pasqualini, H. Huppertz, M. Je, H. Choi and J. Bruns, Triple-Vertex Linkage of (BO_4)-Tetrahedra in a Borosulfate: Synthesis, Crystal Structure, and Quantum-Chemical Investigation of $Sr[B_3O(SO_4)_4(SO_4H)]$, *Angew. Chem., Int. Ed.*, 2021, **60**, 19740–19743, (*Angew. Chem.*, 2021, **133**, 19892–19896).

44 P. Netzsch, F. Pielnhofer and H. A. Höppe, From S–O–S to B–O–S to B–O–B Bridges: $Ba[B(S_2O_7)_2]_2$ as a Model System for the Structural Diversity in Borosulfate Chemistry, *Inorg. Chem.*, 2020, **59**, 15180–15188.

45 P. Netzsch, F. Pielnhofer and H. A. Höppe, From S–O–S to B–O–S to B–O–B Bridges: $Ba[B(S_2O_7)_2]_2$ as a Model System for the Structural Diversity in Borosulfate Chemistry, *Inorg. Chem.*, 2020, **59**, 15180–15188.

46 C. Logemann and M. S. Wickleder, $B_2S_2O_9$: A Boron Sulfate with Phyllosilicate Topology, *Angew. Chem., Int. Ed.*, 2013, **52**, 14229–14232, (*Angew. Chem.*, 2013, **125**, 14479–14482).

47 J. Bruns, H. A. Höppe, M. Daub, H. Hillebrecht and H. Huppertz, Borosulfates—Synthesis and Structural Chemistry of Silicate Analogue Compounds, *Chem. – Eur. J.*, 2020, **26**, 7966–7980.

48 H. A. Höppe, K. Kazmierczak, M. Daub, K. Förg, F. Fuchs and H. Hillebrecht, The First Borosulfate $K_5[B(SO_4)_4]$, *Angew. Chem., Int. Ed.*, 2012, **51**, 6255–6257.

49 M. Daub, K. Kazmierczak, P. Gross, H. Höppe and H. Hillebrecht, Exploring a New Structure Family: Alkali Borosulfates $Na_5[B(SO_4)_4]$, $A_3[B(SO_4)_3]$ (A = K, Rb), $Li[B(SO_4)_2]$, and $Li[B(S_2O_7)_2]$, *Inorg. Chem.*, 2013, **52**, 6011–6020.

50 H. Burzlaff, Die Struktur Des Heidornit, $Ca_3Na_2Cl(SO_4)_2B_5O_8(OH)_2$, *Neues Jahrb. Für Mineral. Monatshefte*, 1967, **1967**, 157–169.

51 H. Yang, Z. Wang, C. Xu, Y. Lin and G. Liu, La2B3O4(OH)3(SO4)2: A new rare-earth borate-sulfate with second-harmonic generation response, *J. Solid State Chem.*, 2023, **317**, 123715.

52 J.-H. Wang, J.-W. Cheng, Q. Wei, H. He, B.-F. Yang and G.-Y. Yang, $NaB_3O_5\cdot 0.5H_2O$ and $NH_4NaB_6O_{10}$: Two Cluster Open Frameworks with Chiral Quartz and Achiral Primitive Cubic Nets Constructed from Oxo Boron Cluster Building Units, *Eur. J. Inorg. Chem.*, 2014, **2014**, 4079–4083.

53 R. Zhang, S. Guo, X. Wang, R. Yang, Z. Chen, W. Zhang, F. Zhang, Z. Guo, S. Han and Z. Yang, Variable dimensionality of the anion framework in four new borophosphates and fluoroborophosphates with short cutoff edges, *Dalton Trans.*, 2022, **51**, 2840–2845.

54 J. Heyd, G. E. Scuseria and M. Ernzerhof, Hybrid functionals based on a screened Coulomb potential, *J. Chem. Phys.*, 2003, **118**, 8207–8215.

55 B.-H. Lei, Z. Yang and S. Pan, Enhancing optical anisotropy of crystals by optimizing bonding electron distribution in anionic groups, *Chem. Commun.*, 2017, **53**, 2818–2821.